# Single-Molecule Magnet Behavior for an Antiferromagnetically Superexchange-Coupled Dinuclear Dysprosium(III) Complex

Jérôme Long,[†,‡] Fatemah Habib,[†,‡] Po-Heng Lin,[†,‡] Ilia Korobkov,[†] Gary Enright,[§] Liviu Ungur,[∥] Wolfgang Wernsdorfer,[⊥] Liviu F. Chibotaru,[∥] and Muralee Murugesu[**,†,‡]

[†]Department of Chemistry, University of Ottawa, 10 Marie-Curie, Ottawa, ON, K1N6N5, Canada

[‡]Centre for Catalysis Research and Innovation, 30 Marie-Curie, Ottawa, ON, K1N6N5, Canada
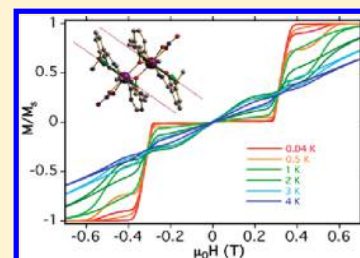
[§]Steacie Institute for Molecular Sciences, NRC, 100 Sussex Drive, Ottawa, ON, K1A0R6, Canada

[∥]Division of Quantum and Physical Chemistry and INPAC—Institute for Nanoscale Physics and Chemistry, Katholieke Universiteit Leuven, Celestijnenlaan, 200F, 3001, Belgium

[⊥]Institut Néel, CNRS and Université J. Fourier, BP 166 25, Avenue des Martyrs, 38042, Grenoble, France

Ⓢ *Supporting Information*

**ABSTRACT:** A family of five dinuclear lanthanide complexes has been synthesized with general formula $[Ln^{III}_2(valdien)_2(NO_3)_2]$ where ($H_2$valdien = $N1,N3$-bis(3-methoxysalicylidene)diethylenetriamine) and $Ln^{III}$ = $Eu^{III}$ **1**, $Gd^{III}$ **2**, $Tb^{III}$ **3**, $Dy^{III}$ **4**, and $Ho^{III}$ **5**. The magnetic investigations reveal that **4** exhibits single-molecule magnet (SMM) behavior with an anisotropic barrier $U_{eff}$ = 76 K. The step-like features in the hysteresis loops observed for **4** reveal an antiferromagnetic exchange coupling between the two dysprosium ions. *Ab initio* calculations confirm the weak antiferromagnetic interaction with an exchange constant $J_{Dy-Dy} = -0.21$ $cm^{-1}$. The observed steps in the hysteresis loops correspond to a weakly coupled system similar to exchange-biased SMMs. The $Dy_2$ complex is an ideal candidate for the elucidation of slow relaxation of the magnetization mechanism seen in lanthanide systems.

## ■ INTRODUCTION

The coordination and supramolecular chemistry of lanthanide ions have been the center of dynamic research, especially for their optical[1] and magnetic properties.[2] In particular, lanthanide coordination complexes have recently attracted much attention in the field of molecular magnetism. Indeed, these systems may hold the key to obtain high anisotropic barrier single-molecule magnets (SMMs).[3] These discrete molecules exhibit superparamagnet-like behavior of slow magnetic relaxation at low temperature. As a consequence, this new class of molecular nanomagnets can be viewed as potential candidates for electronics based on molecules and high-density storage devices.[4]
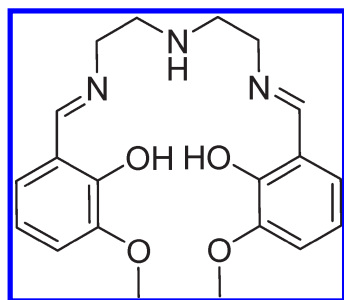
One of the most important issues for technological applications remains the low blocking temperature, $T_B$, observed in SMMs. To date, the largest effective anisotropic barrier reported for a transition-metal SMM is found in a hexanuclear manganese complex with an effective energy barrier of 86 K.[5] This value slightly exceeds the ones observed in the archetype SMMs $[Mn_{12}O_{12}(O_2CR)_{16}(H_2O)_4]$ where $U_{eff}$ < 74 K.[6] While in the case of transition-metal *d* SMMs, the slow relaxation arises from the combination of a large spin ground-state $S$ and an uniaxial anisotropy $D$, the mechanisms involved in pure 4*f* systems are more difficult to grasp. This is mainly due to the fact that, in such systems, the magnetic anisotropy $D$ is much greater than the exchange interaction $J$ between the lanthanide centers (weak exchange limit).[3c]

Retrospectively, the synthesis and study of these pure 4*f* systems has literally been boosted since the discovery that a single-ion lanthanide complex displays slow relaxation of the magnetization.[7] Indeed, the first unquenched orbital moment of some lanthanides ($Tb^{III}$, $Dy^{III}$, $Ho^{III}$) in association with the ligand field leads to high magnetic anisotropy.[8] Interestingly, several relaxations of the magnetization pathways can occur in lanthanide systems, such as direct Orbach[9] or Raman processes.[10] As a proof of concept, the approach of modulating the ligand field has been recently extended to actinide complexes[11] and to a transition-metal complex where slow relaxation of the magnetization has been evidenced.[12] Although considerable efforts have been dedicated to the understanding of the mechanisms in these single-ion SMMs, little attention has been devoted to elucidating the relaxation processes in polynuclear 4*f* SMMs. The main reason lies in the difficulty in correlating the structure to the superparamagnet property. Particularly, it is still difficult to evaluate the real consequence of the lanthanide—lanthanide exchange interaction on the SMM property where the single-ion magnetism seems to be the dominant phenomenon.

The synthetic strategy to obtain polynuclear 4*f* SMMs fundamentally relies on the same concepts as transition-metal SMMs: the use of polydentate bridging ligands which can mediate

**Scheme 1. H₂valdien Ligand**



magnetic interactions between the metallic centers. The choice of the bridging group is critical in the case of lanthanide systems in order to overcome the core nature of $4f$ orbitals and subsequently induce significant exchange interaction between the paramagnetic centers. In addition, the ligand field as well as the coordination geometry strongly influence the local anisotropy of the lanthanide ion. In brief, the interplay between the ligand field effect, the geometry, and the strength of the magnetic interaction between the lanthanide sites will govern the SMM behavior. Taking into account the coordination preference of $4f$ ions for hard Lewis bases (HSAB theory),[13] it is possible to design polytopic ligands in order to direct the assembly of polynuclear lanthanide complexes. Schiff base ligands[14] obtained from the *o*-vanillin moiety have proven to be particularly suitable for the synthesis of $4f$ SMMs.[3a,g,h]

Among the lanthanide family, the Dy[III] ion has indisputably led to the largest number of pure $4f$ SMMs. The explanation resides in the reduced quantum tunneling of the magnetization (QTM) experimentally observed in these systems compared to other lanthanide ions. However, the real physical origin of this behavior remains unclear. The flexibility of the coordination chemistry has been employed to synthesize polynuclear dysprosium(III) complexes with various nuclearities ranging from dinuclear,[3a,k,m] trinuclear,[15] tetranuclear,[3g,16-19] pentanuclear,[3i] and hexanuclear[3l,20,21] to a Dy₂₆ cluster.[22] Nevertheless, in a similar fashion to transition-metal SMMs, the smaller systems tend to present higher anisotropic barriers.[3a,g]

In order to answer the fundamental questions raised previously, model systems are needed. In our efforts to obtain high $T_B$ SMMs as well as understanding the underlying concepts involved, we report here five isostructural dinuclear complexes $[Ln^{III}_2(valdien)_2(NO_3)_2]$ $(Ln^{III} = Eu^{III}$ **1**, $Gd^{III}$ **2**, $Tb^{III}$ **3**, $Dy^{III}$ **4**, $Ho^{III}$ **5**). Compound **4** exhibits a slow relaxation of the magnetization associated with SMM behavior. The characterizations of this SMM property show an antiferromagnetic superexchange coupling between the two Dy[III] centers exhibiting superparamagnetic-like behavior. The simplicity of the symmetric molecular entity allows the evaluation of the exchange interaction between the two Ln[III] ions by computational methods. The observed magnetic properties for all complexes were validated by *ab initio* calculations.

## ■ EXPERIMENTAL SECTION

**Materials.** All manipulations were performed under aerobic/ambient conditions. All chemicals were purchased from Aldrich or Strem Chemicals and used without any further purification.

**Ligand Synthesis.** The ligand, H₂valdien (Scheme 1), (*N1,N3*-bis(3-methoxysalicylidene)diethylenetriamine) was synthesized by mixing *o*-vanillin (0.025 mol) with diethylenetriamine (0.0125 mol) in 40 mL of EtOH. The orange solution was refluxed for 1 h, and after cooling down, the solvent was removed under reduced pressure to afford an orange oil. The latter oil was left to stand overnight to form a yellow precipitate, which was collected by suction filtration and washed with diethyl ether. Yield = 96%. NMR $^1$H (CDCl₃, 400 MHz): $\delta$ 2.97 (*t*, 2H, CH₂—N), 3.69 (*t*, 2H, CH₂—N), 3.88 (*s*, 3H, OCH₃), 6.90 (*t*, 1H, Ar), 6.99 (*d*, 2H, Ar), 8.32 (*s*, 1H, N=CH); $^{13}$C (CDCl₃, 400 MHz): 166.0, 152.1, 148.1, 123.1, 118.6, 117.9, 114.1, 59.3, 56.1, 49.9. Calcd for C₂₀H₂₅N₃O₄: C, 64.67; H, 6.78; N, 11.31. Found: C, 64.59; H, 6.49; N, 11.25. IR (KBr, cm$^{-1}$): 3419, 3056, 2995, 2935, 2900, 2835, 1629, 1468, 1416, 1376, 1335, 1269, 1146, 1128, 1080, 1024, 964, 875, 838, 778, 734.

**Synthesis of [Ln^{III}_2(valdien)_2(NO_3)_2] Complexes.** To a stirred solution of H₂valdien (0.125 mmol, 0.046 g) and Ln(NO₃)₃·6H₂O (0.125 mmol) in 9 mL of MeOH/DMF 2:1 (or MeCN/DMF 2:1 for **2**), triethylamine (0.250 mmol, 35 $\mu$L) was added. The resulting clear yellow solution was stirred for 30 s then filtered. The filtrate was placed into a diethyl ether bath to help crystallization. After 2–3 days, rectangular-shaped yellow crystals were collected. Yields = 55–65%. IR and EA data for all complexes are given in the Supporting Information.

**EA, IR, and NMR Spectroscopy.** Elemental analyses were carried out with a Perkin-Elmer 2400 CHN analyzer. Infrared analyses were obtained using a Nicolet Nexus 550 FT-IR spectrometer in the 4000–650 cm$^{-1}$ range. The spectra were recorded in the solid state by preparing KBr pellets. NMR analyses were conducted on a Bruker Avance 400 spectrometer equipped with an automatic sample holder and a 5 mm auto-tuning broadband probe with Z gradient.

**Single Crystal X-ray Diffraction Studies.** Crystals were grown from a mixture of MeOH/DMF (compounds **1** and **3**–**5**) or MeCN/DMF (**2**) solutions. A single rectangular yellow crystal suitable for X-ray diffraction measurements was mounted on a glass fiber. Unit cell measurements and intensity data collections were performed on a Bruker-AXS SMART 1 k CCD diffractometer using graphite monochromated MoKα radiation ($\lambda$ = 0.71073 Å). The data reduction included a correction for Lorentz and polarization effects, with an applied multiscan absorption correction (SADABS).

The crystal structure was solved and refined using the SHELXTL program suite.[23] Direct methods yielded all nonhydrogen atoms, which were refined with anisotropic thermal parameters. All hydrogen atom positions were calculated geometrically and were riding on their respective atoms. For compound **3**, O(4)—C(20) methoxy group of one ligand is disordered through 36° rotation around C(19)—O(4) axis. Disorder was successfully modeled with the occupational ratio refined as 35:65%.

**Magnetic Measurements.** The magnetic susceptibility measurements were obtained using a Quantum Design SQUID magnetometer MPMS-XL7 operating between 1.8 and 300 K for dc-applied fields ranging from −7 to 7 T. Dc analyses were performed on polycrystalline samples of 13.4, 14.9, 13.5, 6.6, and 7.5 mg of **1**–**5**, respectively, wrapped in a polyethylene membrane (**1**, **2**, **5**) or in grease (**3**, **4**) and under a field ranging from 0 to 7 T between 1.8 and 300 K. Ac susceptibility measurements were carried out under an oscillating ac field of 3 Oe and ac frequencies ranging from 1 to 1500 Hz. The magnetization data were collected at 100 K to check for ferromagnetic impurities that were absent in all samples. Diamagnetic corrections were applied for the sample holder and the core diamagnetism from the sample (estimated with Pascal constants).

**Micro-SQUID Measurements.** Magnetization measurements on oriented single crystals were carried out with an array of micro-SQUIDs.[24] This magnetometer works in the temperature range of 0.04 to ca. 7 K and in fields of up to 0.8 T with sweeping rates as high

5320

dx.doi.org/10.1021/ja109706y |*J. Am. Chem. Soc.* 2011, 133, 5319–5328

**Table 1. Crystallographic Data for Analogous [Ln$^{III}_2$(valdien)$_2$(NO$_3$)$_2$] Complexes**

|  | 1 | 2 | 3 | 4 | 5 |
|---|---|---|---|---|---|
| formula | C$_{40}$H$_{46}$Eu$_2$N$_8$O$_{14}$ | C$_{20}$H$_{23}$GdN$_4$O$_7$ | C$_{40}$H$_{46}$Tb$_2$N$_8$O$_{14}$ | C$_{40}$H$_{46}$Dy$_2$N$_8$O$_{14}$ | C$_{40}$H$_{46}$Ho$_2$N$_8$O$_{14}$ |
| fw | 1166.77 | 588.67 | 1180.69 | 1187.85 | 1192.71 |
| temp. (K) | 200(2) | 200(2) | 200(2) | 100(1) | 200(2) |
| crystal system | triclinic | triclinic | triclinic | triclinic | triclinic |
| space group | P-1 | P-1 | P-1 | P-1 | P-1 |
| a/Å | 10.5977(5) | 10.5766(5) | 10.5536(3) | 10.4807(5) | 10.5104(4) |
| b/Å | 10.6420(5) | 10.5991(5) | 10.5537(3) | 10.5015(5) | 10.5297(4) |
| c/Å | 11.5192(6) | 11.5192(6) | 11.4994(3) | 11.4678(5) | 11.4828(4) |
| α/° | 65.341(2) | 65.1840(10) | 66.1710(10) | 64.937(2) | 66.414(2) |
| β/° | 64.813(2) | 65.4820(10) | 65.0160(10) | 66.519(2) | 65.126(1) |
| γ/° | 80.419(2) | 80.2930(10) | 80.0090(10) | 79.836(2) | 79.981(2) |
| vol/ Å$^3$ | 1068.32(9) | 1066.38(8) | 1061.98(5) | 1048.63(8) | 1056.59(7) |
| Z | 1 | 2 | 1 | 1 | 1 |
| $D_C$/ mg m$^{-3}$ | 1.814 | 1.833 | 1.846 | 1.881 | 1.875 |
| $\mu$/mm$^{-1}$ | 2.986 | 3.160 | 3.381 | 3.614 | 3.795 |
| reflns collected | 19 057 | 10 345 | 8893 | 56 987 | 16 595 |
| R1, wR2 ($I > 2\sigma(I)$)$^a$ | 0.0181, 0.0440 | 0.0215, 0.0532 | 0.0206, 0.0542 | 0.0145, 0.0354 | 0.0130, 0.0347 |
| R1, wR2 (all data) | 0.0194, 0.0447 | 0.0221, 0.0536 | 0.0215, 0.0538 | 0.0155, 0.0358 | 0.0131, 0.0346 |

$^a$ $R = R1 = ||F_o| - |F_c||/|F_o|$; $wR2 = \{[w(F_o^2 - F_c^2)^2]/[w(F_o^2)^2]\}^{1/2}$; $w = 1/[\sigma_2(F_o^2) + (ap)^2 + bp]$, where $p = [\max(F_o^2, 0) + 2F_c^2]/3$; and $Rw = [w(|F_o| - |F_c|)^2/w|F_o|^2]^{1/2}$, where $w = 1/\sigma^2(|F_o|)$.

as 0.28 T·s$^{-1}$ and exhibits field stability of better than $\mu$T. The time resolution is approximately 1 ms. The field can be applied in any direction of the micro-SQUID plane with precision greater than 0.1° by separately driving three orthogonal coils. In order to ensure good thermalization, a single crystal was fixed with apiezon grease.

**Computational Methodology.** The basis sets used for the calculations were taken from the ANO−RCC basis library included in MOLCAS program package.

For magnetic electrons localized in the 4f orbitals of the metal sites the spin−orbit coupling and the crystal field are much stronger than the intramolecular exchange interaction, making these effects a priority in our study. The competition between the spin−orbit coupling, the crystal−field, and the intrinsic multiconfigurational nature of the multielectronic wave function of the 4f electrons can only be treated adequately by an explicitly correlated ab initio method. Therefore, we used a combined approach for studying magnetic properties of complexes 1−5 which implies ab initio calculations of mononuclear lanthanide centers with a model description of the exchange interactions between the centers. This methodology has been already successfully applied for the calculation of the magnetic properties of other polynuclear complexes containing lanthanide and transition-metal ions.[25−27]

The ab initio calculations on individual lanthanide fragments have been carried out with MOLCAS 7.4 program package.[28] In this approach, the relativistic effects are treated in two steps, both based on Douglas−Kroll−Hess Hamiltonian. Scalar terms were included in the basis set generation and used to determine the spin-free wave functions and energies in the multiconfigurational self-consistent field (CASSCF) method. In the second step, spin−orbit interaction was taken into account within the restricted active space state interaction (RASSI) method, which uses the spin free multiconfigurational wave functions as input states. The obtained wave functions and energies of the molecular multiplets were used for the calculation of the anisotropic magnetic properties and the g tensors of the lowest states using a specially designed routine SINGLE−ANISO.[29] As a result, the magnetic properties of a single magnetic ion are calculated by a fully ab initio approach, in which the spin−orbit coupling is considered nonperturbatively.

The exchange interactions between magnetic centers have been included within the Lines model.[30] In this approach, the exchange interaction between different spin terms in the absence of spin−orbit coupling is modeled by a single−parameter isotropic exchange Hamiltonian for each metal pair. This Hamiltonian model is written on the basis of the ab initio computed spin−orbit multiplets of the metal fragments and then diagonalized. The obtained exchange states correspond to the solutions of an anisotropic exchange Hamiltonian of the complex. The advantage of the Lines model is the use of a single parameter to describe the anisotropic exchange interaction for a given pair of interacting metal sites, which in the simplest bilinear approximation is described by 3 × 3 exchange matrix containing nine $J_{ik}$ parameters. The Lines model becomes exact in two limiting cases: (1) isotropic Heisenberg exchange coupling and (2) extremely anisotropic (Ising) exchange coupling. The described approach has been implemented in the computer program POLY−ANISO,[36] which is interfaced with the routine SINGLE−ANISO. The obtained exchange spectrum and eigenfunctions were used to calculate the magnetic properties of the dinuclear complexes.

## ■ RESULTS AND DISCUSSION

**Synthesis and Structural Analysis.** The compartmental acyclic Schiff base H$_2$valdien ligand is obtained from the condensation reaction of o-vanillin and diethylenetriamine. This ligand displays two distinct coordination pockets which can encapsulate lanthanide centers. The large size of the inner compartment, formed by the donor set N$_3$O$_2$, is particularly appropriate to accommodate a sizable 4f ion. Only a few examples of coordination complexes are reported with H$_2$valdien.[31] In 2007, Dou et al. structurally characterized two mononuclear complexes with large La$^{III}$ and Nd$^{III}$ ions where only the outer donor O$_4$ set of H$_2$valdien was involved in the coordination.[31b] Moreover, in some cases, ortho positions on the aromatic rings are substituted with methoxy groups in order to prevent the formation of bridged complexes;[31b] however, in our synthetic methodology we employed the latter functionality to
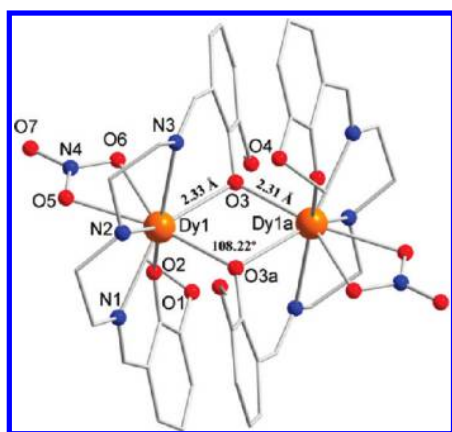
**Figure 1.** The molecular structure of $[Dy^{III}_2(valdien)_2(NO_3)_2]$, **4**. Color code: orange (Dy), red (O), blue (N), and grey (C). Hydrogen atoms have been omitted for clarity.

**Table 2. Selected Bond Distances and Angles**

| $Ln^{III}$ | $Ln^{III}-Ln^{III}$ (Å) | $Ln^{III}-O3$ (Å) | $Ln^{III}-O3-Ln^{III}$ (°) |
|---|---|---|---|
| $Eu^{III}$ | 3.830(3) | 2.374(3)−2.383(3) | 107.26(6) |
| $Gd^{III}$ | 3.811(1) | 2.347(3)−2.371(2) | 107.76(8) |
| $Tb^{III}$ | 3.788(1) | 2.330(2)−2.351(2) | 108.05(8) |
| $Dy^{III}$ | 3.768(3) | 2.317(2)−2.334(3) | 108.22(3) |
| $Ho^{III}$ | 3.754(3) | 2.307(2)−2.328(3) | 108.17(5) |

promote coordination in both pockets. The stoichiometric reaction of $H_2$valdien and $Ln(NO_3)_3 \cdot 6H_2O$ in the presence of an organic base (NEt$_3$, 2 equiv) in a MeOH/DMF mixture (or $CH_3CN$/DMF for **2**) affords the crystallization of the five dinuclear compounds $[Ln^{III}_2(valdien)_2(NO_3)_2]$ ($Ln^{III}$ = $Eu^{III}$ **1**, $Gd^{III}$ **2**, $Tb^{III}$ **3**, $Dy^{III}$ **4**, $Ho^{III}$ **5**). Slight variation in metal to ligand ratio still gave the same complexes.

The single X-ray crystallography studies reveal that all five compounds are isostructural and crystallize in the triclinic *P-1* space group (Table 1). As an example, the structure of the dysprosium analogue, compound **4**, will be described (Figure 1). The asymmetric unit consists of one $Dy^{III}$ ion, one valdien$^{2-}$ ligand and a nitrate ion. The centrosymmetric dinuclear complex is composed of two eight-coordinate $Dy^{III}$ ions bridged by phenoxo groups (O3, O3a) of the valdien$^{2-}$ ligands with a Dy1−O3−Dy1a angle of 108.22(3)° and a Dy−Dy distance equal to 3.768(3) Å. The central core $Dy_2O_2$ appears to be nearly rhombic, the two Dy−O3 distances being 2.31 and 2.33 Å. One terminal phenoxo group coordinates the dysprosium ion with a short distance Dy−O2 of 2.19 Å. Interestingly, the methoxide groups are not involved in the coordination of the lanthanide centers and thus remain strictly in the flexible inner $N_3O_2$ compartment of the ligand. In contrast with the previously reported mononuclear complexes based on $La^{III}$ and $Nd^{III}$,[31b] the inner $N_3O_2$ compartment is more adequately sized for the encapsulation of smaller lanthanide ions, such as $Dy^{III}$. Moreover, the dimerization of the molecule is most likely due to the presence of NEt$_3$ as base promoting the full deprotonation of $H_2$valdien, which subsequently provide phenoxides as bridging groups. The coordination sphere is completed by a bidentate nitrate ion leading to an overall $N_3O_5$ coordination environment. The centrosymmetry of the complex leads to the absence of a

**Table 3. Lanthanide Geometry Analysis by SHAPE Software**

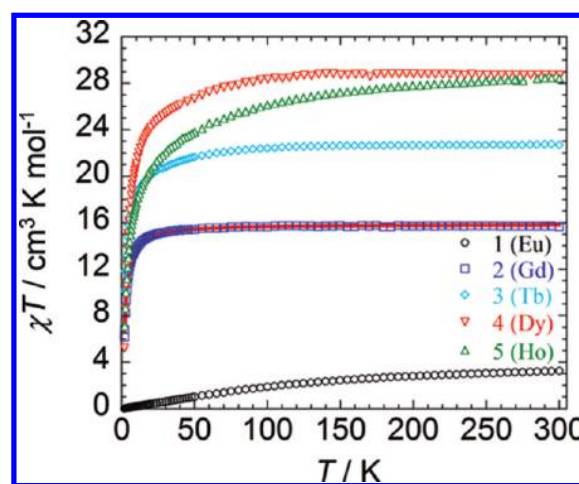| $Ln^{III}$ | square antiprism ($D_{4d}$) | dodecahedron ($D_{2d}$) |
|---|---|---|
| $Eu^{III}$ | 4.38503 | 2.37483 |
| $Gd^{III}$ | 4.26909 | 2.18035 |
| $Tb^{III}$ | 4.30761 | 2.02714 |
| $Dy^{III}$ | 4.20132 | 1.90380 |
| $Ho^{III}$ | 4.24485 | 1.89277 |



**Figure 2.** Temperature dependence of the $\chi T$ product at 1000 Oe for complexes **1**−**5** (with $\chi$ being the molar susceptibility per dinuclear complex defined as $M/H$). The solid line corresponds to the best fit for **2**.

dihedral angle between the planes defined by the atoms O3−Dy1−O3a and O3−Dy1a−O3a. Despite the isostructurality, small differences appear between the five dinuclear compounds (Table 2). For instance, the general trend observed is a decrease of the intramolecular $Ln^{III}-Ln^{III}$ distance from $Eu^{III}$ to $Ho^{III}$ (3.830(3) to 3.762(6) Å), while the bridging $Ln^{III}-O3-Ln^{III}$ angle increases slightly (Table 2). In the case of lanthanides, the geometry of the metallic center is strongly correlated to the local anisotropy of the paramagnetic ion. Thus, a systematic analysis of the coordination geometry must be performed. With this in mind, exact geometry of the octacoordinated lanthanide ions was determined using the SHAPE[32] software. Close analysis of the resulting data reveals that the values obtained differ from zero (which represents the case of the ideal geometry considered). Therefore, an intermediate geometry between square antiprism ($D_{4d}$) and dodecahedron ($D_{2d}$) is observed for all complexes (Table 3 and Figure S1, Supporting Information). The slight variation observed along the family can be directly correlated to the general decrease of the ionic radius of the lanthanide ion from $Eu^{III}$ to $Ho^{III}$ (Figure S2, Supporting Information). Moreover, the intermediate/distorted geometry seen even for $Gd^{III}$ might lead to non-negligible local magnetic anisotropy. The latter assumption can be verified by the comparison of the coupling constants ($J$) obtained by fitting the susceptibility data using an isotropic model with calculated $J$ value from an anisotropic model (*vide infra*).

An intramolecular H-bond appears between N2−H and the methoxide oxygen (O4) with a distance of 2.11 Å and an angle of 165.8°, close to linearity (Figure S3, Supporting Information). The analysis of the packing arrangement (Figures S4−S6,
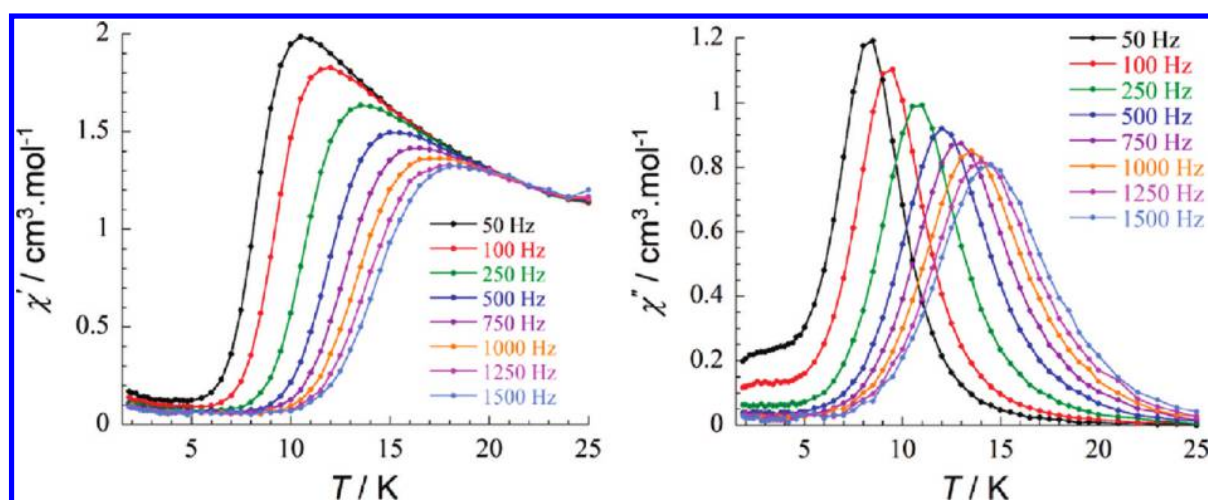
**Figure 3.** Temperature dependence of the in-phase $\chi'$ (left) and out-of-phase $\chi''$ (right) ac susceptibility signals under zero dc field for **4**.

Supporting Information) reveals the shortest intermolecular Dy$\cdots$Dy distance of 7.36 Å, confirming the spatial isolation of the dinuclear units.

**Magnetic Properties.** The dc magnetic properties of compounds **1**–**5** were investigated under a 1000 Oe field in the temperature range 1.8–300 K (Figure 2). Field dependence of the magnetization for all complexes between 1.8 and 8 K are shown in Figures S7–S12, Supporting Information. For all compounds, the observed paramagnetism arises uniquely from the 4f Ln$^{III}$ ions. At room temperature, the $\chi T$ values of complexes **1**–**5** are 3.2, 15.7, 22.7, 28.7, and 28.4 cm$^3 \cdot$K$\cdot$mol$^{-1}$, respectively. These values are in good agreement with the expected theoretical values (**2**: 15.76; **3**: 23.63; **4**: 28.34; **5**: 28.16 cm$^3 \cdot$K$\cdot$mol$^{-1}$) for two noninteracting lanthanide ions: Gd$^{III}$ ($^8S_{7/2}$, $S = 7/2$; $L = 0$, $g = 2$, $C = 7.88$ cm$^3 \cdot$K$\cdot$mol$^{-1}$), Tb$^{III}$ ($^7F_6$, $S = 3$, $L = 3$, $g = 3/2$, $C = 11.82$ cm$^3 \cdot$K$\cdot$mol$^{-1}$), Dy$^{III}$ ($^6H_{15/2}$, $S = 5/2$, $L = 5$, $g = 4/3$, $C = 14.17$ cm$^3 \cdot$K$\cdot$mol$^{-1}$) and Ho$^{III}$ ($^5I_8$, $S = 2$, $L = 6$, $g = 5/4$, $C = 14.08$ cm$^3 \cdot$K$\cdot$mol$^{-1}$). Due to the presence of thermally populated excited states, the magnetic properties of the europium analogue **1** remain difficult to interpret even at room temperature. However, the typical nonmagnetic ground state ($^7F_0$) is observed at low temperatures as suggested by the $\chi T$ value of 0.04 cm$^3 \cdot$K$\cdot$mol$^{-1}$ at 1.8 K.[33]

The strength of the magnetic interaction between the two lanthanide ions in the dinuclear complexes can be easily quantified with the gadolinium analogue **2**. Indeed, the Gd$^{III}$ ions present no spin–orbit coupling at the first order. Thus, the decrease of the $\chi T$ when lowering the temperature for **2** reveals directly the presence of an antiferromagnetic interaction between the Gd$^{III}$ ions. Application of the van Vleck equation to the Kambe's vector coupling scheme by using the isotropic spin Hamiltonian H $= -JS_a \cdot S_b$ with $S_a = S_b = 7/2$, it is possible to reproduce the variation of $\chi T$ vs $T$. The best-fit parameters obtained are $J = -0.178(1)$ cm$^{-1}$ and $g = 2.00(0)$. As expected for pure lanthanide systems, the exchange interaction is rather weak as a consequence of the shielded $f$ orbitals that have little overlap with bridging ligand orbitals. Although the obtained values are in good agreement with the reported coupling constants for other phenoxo-bridged Gd$^{III}$ systems,[34] especially for centrosymmetric complexes,[35,36] it is important to verify that the lowered symmetry of the Gd$^{III}$ ion (Table 3) in **2** might lead to non-negligible zero-field splitting (ZFS). The latter can also
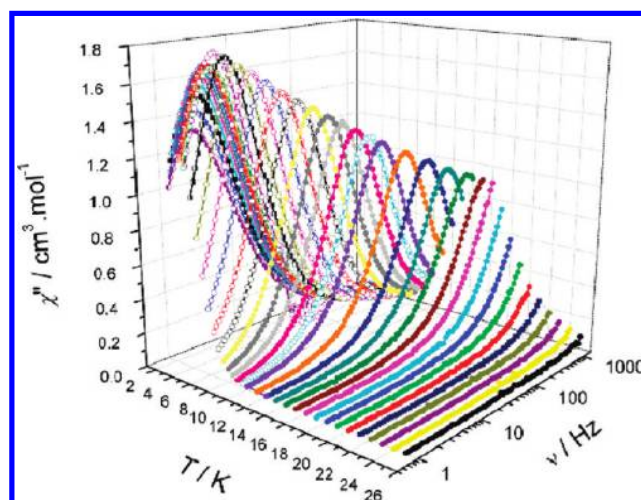


**Figure 4.** Out-of-phase susceptibility $\chi''$ vs frequency $\nu$ (logarithmic scale) in the temperature range 2–25 K for **4**.

contribute toward the negative deviation of the $\chi T$ at low temperature. This will be verified using *ab initio* calculations (*vide infra*).

Magnetization measurements performed at low temperatures reveal a saturation of 13.46 $\mu_B$ at 7 T, in good agreement with the expected theoretical value of 14.00 $\mu_B$ ($g = 2.00$). The solid line corresponding to the Brillouin function for two uncoupled spins $S = 7/2$ ($g = 2.00$) is slightly higher than the magnetization curve of **2**. This may confirm that the antiferromagnetic interaction is operative (Figures S7 and S9, Supporting Information). However, *ab initio* calculation results show that the isotropic exchange interaction is overestimated. This could arise from the presence of non-negligible ZFS that results in larger isotropic $J$ values (see Computational Section).

For compounds **3**–**5**, the thermal variation of $\chi T$ shows a negative deviation upon cooling to reach a value of 10.2, 5.2, and 7.1 cm$^3 \cdot$K$\cdot$mol$^{-1}$ at 1.8 K for compounds **3**–**5**, respectively (Figure 2). For such lanthanide ions with an unquenched orbital moment associated with a ligand field, the decrease of the $\chi T$ can originate from the following possible contributions: (i) antiferromagnetic interactions between the lanthanide centers; (ii) the

5323

dx.doi.org/10.1021/ja109706y |*J. Am. Chem. Soc.* 2011, 133, 5319–5328
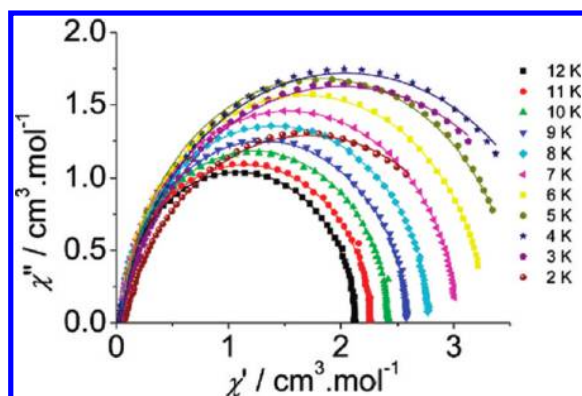
**Figure 5.** Cole−Cole (Argand) plot for **4** obtained using the ac susceptibility data. The solid lines correspond to the best fit obtained with a generalized Debye model.
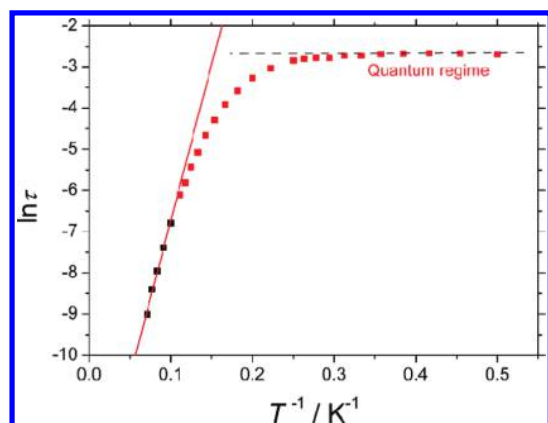


**Figure 6.** Relaxation time of the magnetization $\ln(\tau)$ vs $T^{-1}$ (Arrhenius plot using ac data) for **4**. The line corresponds to the fit.



**Figure 7.** Field dependence of the normalized magnetization of **4** between 0.04 and 4 K for dc applied field ranging from −1.5 to 1.5 T.



**Figure 8.** Sweep rate dependence of the normalized magnetization of **4** at 0.04 K for dc applied field ranging from −1.5 to 1.5 T.

thermal depopulation of the Stark sublevels; and (iii) the presence of significant magnetic anisotropy.

The thermally populated diamagnetic ground state ($^7F_0$) of the europium analogue **1** leads to a value of the magnetization close to zero even at 7 T. For compounds **3**−**5**, the high field linear variation and non-saturation of the magnetization indicate the presence of significant magnetic anisotropy and/or low-lying excited states (Figure S7, Supporting Information). The values of the magnetization at 7 T are 10.5, 11.6, and 10.3 $\mu_B$ for compounds **3**−**5**, respectively. The significant deviation from the expected magnetization saturation values indicates a strong contribution from the ligand field. However, the value obtained for compound **4** is close to the value of 5.23 $\mu_B$ per Dy$^{III}$ ion in a crystal field environment.[3b,37]

In order to investigate the presence of slow relaxation of the magnetization which may originate from an SMM behavior, ac measurements were performed on all complexes in the temperature range 1.8−25 K with zero dc field and a 3 Oe ac field at frequencies between 50 and 1500 Hz. The temperature and frequency dependent ac susceptibility signal was observed below 25 K for the dysprosium analogue **4** (Figure 3). All other complexes did not exhibit such signals. The out-of-phase ($\chi''$) component of the ac susceptibility (Figure 3 right) clearly exhibits a frequency dependent full peak with one maximum.
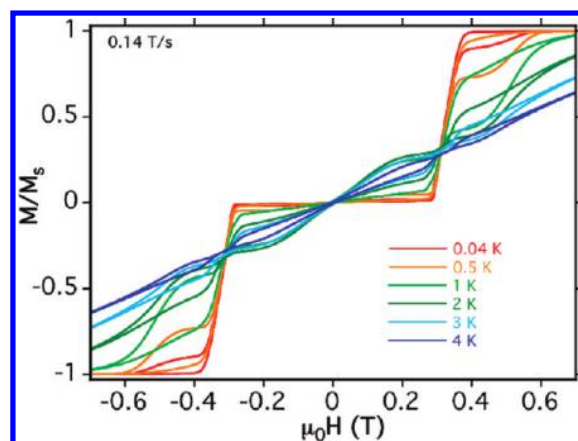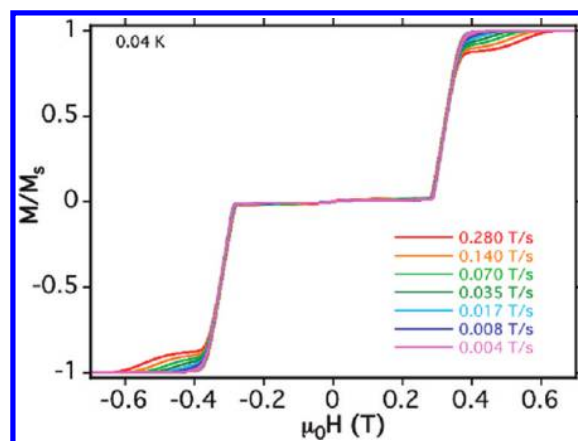
Additionally, a frequency dependence of the maximum associated only with a single relaxation process appears clearly on a tridimensional plot of the variation of $\chi''$ versus the temperature and the frequency of the oscillating field between 1 and 1500 Hz (Figure 4). This indicates slow relaxation of the magnetization associated with SMM behavior.

Such single peak relaxation behavior is remarkable as most lanthanide systems exhibit multiple relaxation processes due to significant quantum tunneling at zero field and/or to the presence of crystallographically independent lanthanide centers.[3g,21] Here, the presence of a single relaxation process agrees with the presence of a unique crystallographic Dy$^{III}$ ion in the dinuclear structure. A close inspection of the latter relaxation process in the tridimensional plot reveals two regimes of relaxation (Figure 4). For temperatures higher than 4 K, the system follows a thermally activated relaxation process. However, below 4 K, the relaxation becomes temperature independent (i.e., quantum regime), and a drop of the imaginary susceptibility, $\chi''$, is observed. The latter regime most likely originates from an antiferromagnetic interaction between the Dy$^{III}$ ions which tends to create a nonmagnetic ground state with decreasing temperature.[15] The graphical representation of $\chi''$ vs $\chi'$ (Cole−Cole plot[38]) in the temperature range 2−12 K further confirms the single relaxation process (Figure 5). For temperatures higher than 4 K, symmetric
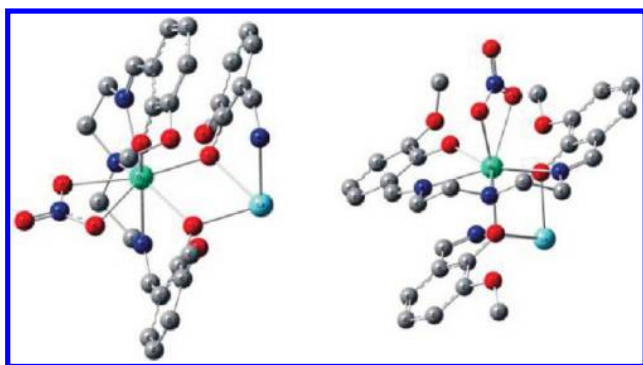
**Figure 9.** Two views of the structure of the calculated mononuclear lanthanide fragment of **4**. The structure of the fragments of **1**−**3** and **5** are similar.



**Figure 10.** A comparison of the experimental and calculated (solid line) magnetic susceptibility for complex **1**−**5**.

semicircles are obtained. The data can be fitted using a generalized Debye model.[39] The α parameter, indicating deviation from the pure Debye model, is lower than 0.03 for this temperature range. This low degree of disorder confirms that the magnetization relaxes with a unique single characteristic time. When the system enters the quantum regime (below 4 K), a slight asymmetry in the Cole–Cole plot appears as well as an increase in α up to 0.18 (2 K) is observed. This indicates a narrow width of the distribution in this single relaxation process. As observed for the frequency dependent ac susceptibility, the antiferromagnetic interaction between the two $Dy^{III}$ ions results in a drop of the out-of-phase susceptibility, $\chi''$, in the Cole–Cole plot.

The anisotropic energy barrier, $U_{eff}$ can be obtained from the high-temperature regime of the relaxation where it is thermally induced (Arrhenius law, $\tau = \tau_0 \exp(U_{eff}/kT)$). The effective energy barrier obtained from fitting (Figure 6) is $U_{eff} = 76$ K ($\tau_0 = 6.04 \times 10^{-7}$ s), which is comparable in magnitude to the archetype $Mn_{12}$−Ac SMM.[6]

In order to reduce the quantum tunneling effects frequently associated with lanthanide SMMs, ac measurements in the presence of a static dc field were carried out. Interestingly, no significant shift in the maximum position was observed for dc fields up to 2000 Oe. This suggests that the tunneling below the latter field is less efficient. To further probe this, various magnetic measurements on diluted samples are currently being investigated.

The SMM behavior can be further investigated through micro-SQUID experiments between 0.04 and 4 K (Figures 7 and 8). Hysteresis loops were measured on eas*y* axis-oriented single crystals. An "S-shaped" hysteresis is observed with a large step at $H = \pm 0.3$ T, which can be directly associated with a spin flip of the antiferromagnetically coupled $Dy^{III}$ spins. Moreover, the strong sweep-rate dependence confirms the presence of quantum tunneling of the magnetization. The tunnel position resonance shift at ±0.3 T is due to each $Dy^{III}$ ion acting as bias field on its neighboring metal ion within the molecule. Such behavior is similar to previously observed $\{Mn_4\}_2$ systems where two cluster units are entangled in their slow relaxation of the magnetization.[40] It can therefore be concluded that for **4** the hysteresis loops reveal exchange-biased interactions between the two individually relaxing $Dy^{III}$ ions. The strength of this weak exchange coupling determined through low-temperature dc measurements corresponds to 0.32 T. In addition to the unique aforementioned behavior, complex **4** reveals an atypical behavior: Below 1 K the coercive field increases with increasing temperature, contrary to what is usually observed in SMMs and traditional magnets. This can be ascribed to strong
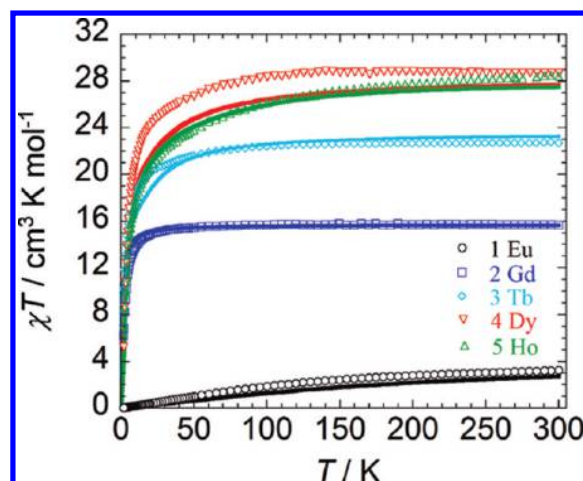
tunneling at the steps, which is reduced by thermal activations around the corresponding tunnel splitting.

## ■ *AB INITIO* CALCULATIONS AND SIMULATIONS OF MAGNETISM

**Computational Details.** The following contractions were used: $[8s7p5d4f2g1h]$ for lanthanide ions, $[4s3p2d]$ for close O and N, $[3s2p]$ for distant O, N, and for all C, and $[2s]$ for H. The active space of the complete active space self-consistent field (CASSCF) method included all $4f$ electrons of the corresponding lanthanide ion spanning seven orbitals. A good description of the spin−orbit coupling on the metal sites usually requires the mixing of a large number of states. In the present case we have mixed the maximum number of spin-free states which was possible with our hardware (Eu, 215; Tb, 215; Gd, 262; Dy, 279; Ho, 316). The free ion parentage of these states, their spin−orbit energies, and the local magnetic axes of the individual fragments can be found in Supporting Information in Tables S1−S5. The latest implementations of the MOLCAS *ab initio* methodology[41] (Choleski decomposition of the bielectronic integrals, parallelization, etc.) allow the treatment of relatively large mononuclear fragments. The structure of the calculated fragments is shown in Figures 9 and S13 − S17, Supporting Information.

To confirm the observed dc magnetic behavior, *ab initio* calculations were performed for all isolated complexes. The temperature-dependent magnetic susceptibility results for all complexes are shown in Figure 10. A comparison of the experimental and calculated molar magnetization at 2 K for all complexes is given in Figure 11. In the case of complex **1**, $Eu^{III}$ is a non-Kramers ion with a nonmagnetic ground state $^7F_0$. The unusually large experimental $\chi T_{300\,K} = 3.2$ cm$^3$·K·mol$^{-1}$ can be explained by a large temperature-induced paramagnetism (TIP) and the thermal population of excited multiplets.

The energy spectrum of **1** for several low-lying excited states is shown in Table 4. The energy of the first excited multiplet is already much lower than the free ion value (400 cm$^{-1}$) which is the reason for the enhanced susceptibility in **1**. As the table shows, the stabilization energy of the ground spin−orbital singlet is a function of the number of spin-free states included in the spin−orbit coupling calculation. A good agreement with
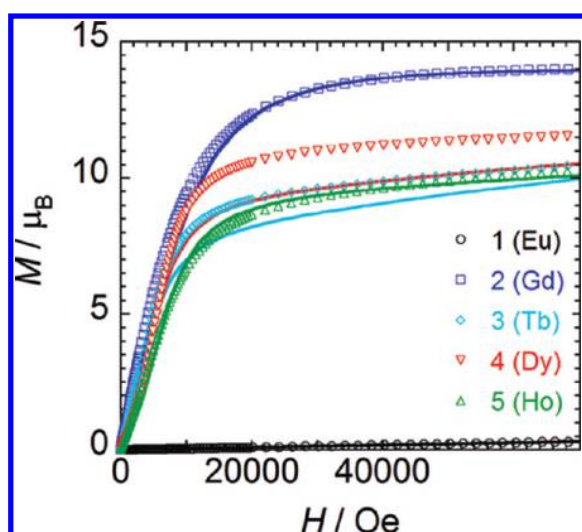
5325

dx.doi.org/10.1021/ja109706y |*J. Am. Chem. Soc.* 2011, 133, 5319–5328

**Figure 11.** A comparison of the experimental and calculated (solid lines) molar magnetization for complexes **1**–**5**.

**Table 4. Lowest Multiplets of the Eu$^{III}$ Fragment**[a]

| no. | A | B | C |
|---|---|---|---|
| 1 | 0.000 | 0.000 | 0.000 |
| 2 | 101.860 | 208.547 | 231.432 |
| 3 | 273.267 | 378.847 | 401.711 |
| 4 | 429.725 | 531.867 | 554.371 |
| 5 | 628.622 | 899.761 | 941.396 |
| 6 | 676.208 | 960.062 | 1002.795 |
| 7 | 802.393 | 1078.854 | 1121.218 |
| 8 | 859.612 | 1139.114 | 1181.665 |
| 9 | 874.699 | 1156.185 | 1199.146 |
| 10 | 1392.231 | 1856.677 | 1905.155 |

[a] A: spin-free states originating from $^7F$ multiplet were mixed by spin–orbit coupling. B: states coming from $^7F$, $^5D$, $^5L$, $^5G$, $^5H$, $^5I$, $^5F$, $^5K$, $^5G$, and $^5D$ multiplets were mixed by spin–orbit coupling. C: states coming from $^7F$, $^5D$, $^5L$, $^5G$, $^5H$, $^5I$, $^5F$, $^5K$, $^5G$, $^5D$, $^3P$, $^3O$, $^3M$, $^3K$, $^3H$, $^3F$, $^3I$, and $^1Q$ multiplets were mixed by spin–orbit coupling.

experimental data is obtained if the energy of the first excited multiplet in the set C is reduced by 40% (Figure S18, Supporting Information).

The apparent overestimation of the excitation energy(ies) is probably related to the fact that the CASSCF wave function is too "ionic" due to the lack of dynamical correlation. These effects can be accounted for by performing a multistate CASPT2 calculation. However, due to large basis of RASSI states need to be taken into account for a good description of the spin–orbit coupling on the lanthanide ions, the multistate CASPT2 was computationally too costly.

In the case of gadolinium analogue **2** the simulated magnetism with the Lines parameter gave $J_{Gd-Gd} = -0.08$ cm$^{-1}$, corresponding to $S = 7/2$, (Figures 10 and 11 and Figure S19 Table S2, Supporting Information). Contrary to the description based on the isotropic exchange model (Figures 2 and S7, Supporting Information), the simulations in Figures 10 and 11 fit very well both the susceptibility and the magnetization. The important ingredient brought by *ab initio* calculations is the zero-field
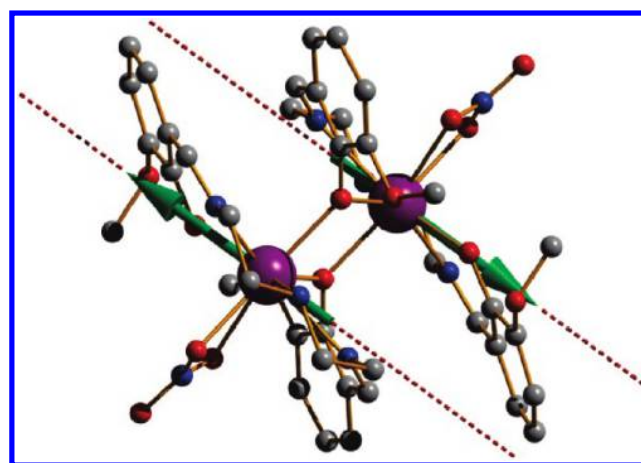
splitting of the ground $S = 7/2$ term on each Gd$^{III}$ site, which appears to be non-negligible (Table S2, Supporting Information). The noticeable difference between the fitted lines exchange parameter, $J_{Gd-Gd} = -0.08$ cm$^{-1}$, and the fitted parameter of isotropic exchange interaction, $J_{isotropic} = -0.178$ cm$^{-1}$, is due to this zero-field splitting. The latter ZFS arises most likely from the lowered symmetry of Gd$^{III}$ ions as seen in Table 3. Considering smaller splittings of the ground $^8S_0$ multiplet in the Lines model resulted in larger fitted values for the exchange parameter.

For the analogous Tb$_2$ complex **3**, from the basis set of column 3, Table S3, Supporting Information, the Lines parameter of $J_{Tb-Tb} = -0.1$ cm$^{-1}$ was obtained, and the experimental and fitting data can be seen in Figures 10 and 11, and Figure S20 (Supporting Information). Although the obtained fit is reasonable, the experimental susceptibility obtained is slightly lower than the calculated one at 300 K. This slight difference between the experimental and the calculated magnetic susceptibility and magnetization remains unclear.

The simulated magnetism of complex **4** with the Lines parameter $J_{Dy-Dy} = -0.21$ cm$^{-1}$ is shown in Figures 10 and 11, and the simulations correspond to the basis set of column 5 from Table S4, Supporting Information. The calculated directions of the anisotropy axes and the local magnetic moments in one of the two-fold degenerate Ising ground states are shown in Figure 12.

Due to the inversion symmetry of complexes **1**–**5**, the orientation of the local anisotropy axes is strictly parallel, while the local magnetic moments in both Ising ground states are antiparallel to each other. At high temperature (300 K), the value of $\chi T$ is well approximated by the sum of the contributions of individual centers. The experimental susceptibility obtained is slightly higher than the calculated one at 300 K. A reduction of 8% in both experimental magnetic susceptibility and molar magnetization is in good agreement with the calculated curves (Figure S21, Supporting Information).

Finally, the simulated magnetism of Ho$_2$ complex (**5**) with the Lines parameter $J_{Ho-Ho} = -0.44$ cm$^{-1}$ is shown in Figures 10 and 11, and Figure S22 (Supporting Information). The simulations correspond to the basis set of column 2 from Table S5, Supporting Information. The agreement with experimental susceptibility and magnetization is very good.



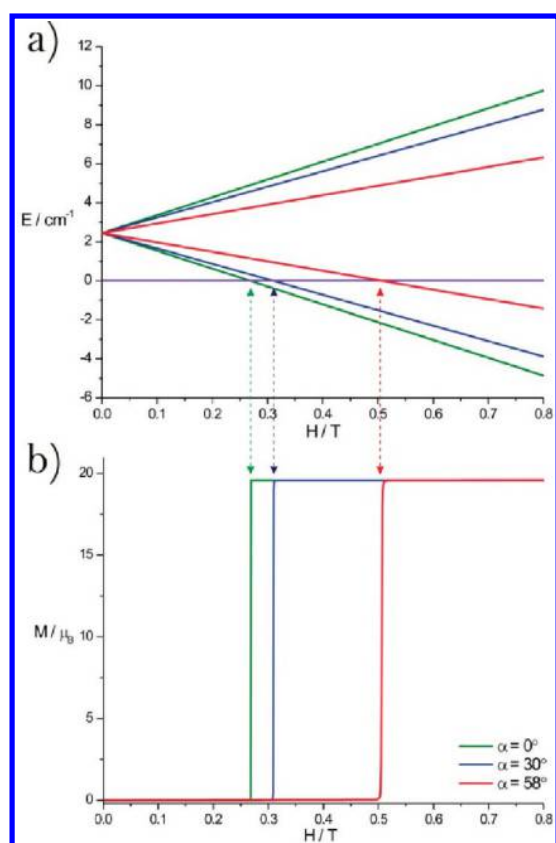**Figure 12.** Orientation of the local main magnetic axes of the ground Kramers doublet in **4**. In Tb$_2$ (**3**) and Ho$_2$ (**5**) complexes, the orientation of the main magnetic axis is analogous.

5326

dx.doi.org/10.1021/ja109706y |*J. Am. Chem. Soc.* 2011, 133, 5319–5328

**Figure 13.** Zeeman spectrum (a) and simulated magnetization curve (b) at $T = 0$ K for **4**.

**Table 5. Calculated Exchange Coupling Constants for Dinuclear Complexes 1−5**

| $Ln^{III}$ | $Ln^{III}-Ln^{III}$ (Å) | $Ln^{III}-O3-Ln^{III}$ (°) | $J_{calc}-Lines$ (cm$^{-1}$) | $J_{calc}-Ising$ (cm$^{-1}$) |
|---|---|---|---|---|
| $Eu^{III}$ | 3.830(3) | 107.26(6) | − | − |
| $Gd^{III}$ | 3.811(1) | 107.76(8) | −0.08 | − |
| $Tb^{III}$ | 3.788(1) | 108.05(8) | −0.10 | −3.60 |
| $Dy^{III}$ | 3.768(3) | 108.22(3) | −0.21 | −5.25 |
| $Ho^{III}$ | 3.754(3) | 108.17(5) | −0.44 | −7.04 |

Information as 165 K. Interestingly, this value does not match the anisotropic barrier derived from the ac measurements ($U_{eff}$ = 76 K). Despite the fact that the relaxation time follows a thermally activated behavior at high temperature, the energy differences observed indicate that an Orbach process might not be predominant and that further relaxation pathways have to be considered. Another reason for this discrepancy can be the overestimated excitation energies of the local Dy multiplets obtained within the CASSCF approximation.

## ■ CONCLUSION AND OUTLOOK

Using a compartmental Schiff base ligand based on the *o*-vanillin motif, a family of centrosymmetric dinuclear lanthanide complexes has been synthesized and fully characterized. For all complexes, an antiferromagnetic interaction between the lanthanide ions is observed. Furthermore, computational methods allow us to validate observed experimental behavior. Simulations based on *ab initio* calculations predict that the strength of the interaction increases with the decrease of the intramolecular $Ln^{III}-Ln^{III}$ distances as well as the increase in the bridging $Ln^{III}-O3-Ln^{III}$ angle. Due to the fast relaxation of the magnetization for $Tb^{III}$ and $Ho^{III}$ analogues, only the $Dy^{III}$ analogue, **4**, exhibits a slow relaxation of the magnetization associated with SMM behavior and an anisotropic barrier of $U_{eff}$ = 76 K. The single relaxation process observed adequately correlates with the presence of a unique crystallographic $Dy^{III}$ ion. Although the observed slow magnetic relaxation is mainly due to the single-ion relaxation, the results above demonstrate that a weak exchange coupling ($J = -0.21$ cm$^{-1}$) between the lanthanide ions affects the QTM. Therefore, the observed steps in the hysteresis loops correspond to a weakly coupled system similar to exchange-biased SMMs.[40] Due to the centrosymmetry and simplicity of the system, complex **4** can be viewed as an ideal model for understanding the parameters that affect the SMM behavior in polynuclear 4f systems. Even though the coupling between the lanthanide ions remains small through the superexchange pathway, it is important to investigate simple analogous dinuclear systems to understand the nature and the strength of the interaction. Subsequently, their effect on the relaxation mechanism involved in weakly coupled molecules can be investigated. By modulating the superexchange pathway the nature and the strength of the interaction can be further tuned. We believe this may be the way forward for controlling the interactions between 4f ions and designing better SMMs.

## ■ ASSOCIATED CONTENT

**ⓢ Supporting Information.** Detailed description of the computation data, packing diagrams, SHAPE, infrared data, and

The general trend, which can be inferred from these simulations, is the increase of the exchange interaction when the intramolecular $Ln^{III}-Ln^{III}$ distance decreases (Table 5). This is consistent with previously reported studies on the dinuclear gadolinium complexes.[34] However, the change of the orbital overlap between the *f* centers, caused by an increase of the bridging angle, could also lead to the increase of the exchange interaction. It is noteworthy that the coupling constant increases with the addition of *f* electrons along with the *f*-orbital contraction down the series. Further investigation is needed to confirm such trends.

In order to better characterize the distinct SMM behavior observed for **4**, several approximations were tested (Table S4, Supporting Information). In the largest computational approximation (see Supporting Information) the complete molecule was kept as is. The only change was the substitution of the neighboring $Dy^{III}$ ion with diamagnetic $La^{III}$ simulated in the *ab initio* calculations by the same ANO-RCC all-electron basis set as used for $Dy^{III}$. The obtained *g* tensor is strongly anisotropic ($g_z$ = 19.547) pointing to an Ising interaction between $Dy^{III}$ ions. The orientations of the magnetic axes are found to be almost collinear to the shortest Dy−O2 distance with an angle of 4.05°.

The simulated magnetization curve at 0 K (Figure 13) shows a single magnetization step at a value of applied field strongly dependent on its angle with the anisotropy axes of the $Dy^{III}$ ions. For instance, the observed jump at 0.3 T in the micro-SQUID experiment (Figure 8) requires a large angle of 58° between the anisotropy axes and the applied magnetic field.

The energy of the first excited Kramers doublet on each $Dy^{III}$ fragment is obtained with the set 5 in Table S4, Supporting

5327

dx.doi.org/10.1021/ja109706y |*J. Am. Chem. Soc.* 2011, 133, 5319–5328

CIF files for all complexes. This material is available free of charge via the Internet at http://pubs.acs.org.

# ■ AUTHOR INFORMATION

**Corresponding Author**

*m.murugesu@uottawa.ca.

# ■ REFERENCES

(1) (a) Binnemans, K. *Coord. Chem. Rev.* **2009**, *109*, 4283. (b) Faulkner, S.; Natrajan, L.; William, S.; Sykes, D. *Dalton Trans.* **2009**, *20*, 3890. (c) Bünzli, J.-C.; Piguet, C. *Chem. Soc. Rev.* **2005**, *34*, 1048. (d) Tsukube, H.; Shinoda, S. *Chem. Rev.* **2002**, *102*, 2389. (e) Parker, D.; Dickins, R. S.; Puschmann, H.; Cossland, C.; Howard, J. A. K. *Chem. Rev.* **2002**, *102*, 1977. (f) Ward, M. D. *Coord. Chem. Rev.* **2007**, *251*, 1663. (g) Dos Santos, C. M. G.; Harte, A. J.; Quinn, S. J.; Gunnlaugsson, T. *Coord. Chem. Rev.* **2008**, *252*, 2512.

(2) Binnemans, K. . *Handbook on the Physics and Chemistry Lanthanides of Rare-Earth*; Gschneidner, K. A. Jr, Bünzli, J.-C. G., Pecharsky, V. K., Ed.; Elsevier: Amsterdam, The Netherlands, 2005; Vol. 35, Chapter 225, p 107.

(3) (a) Lin, P.-H.; Burchell, T. J.; Clérac, R.; Murugesu, M. *Angew. Chem., Int. Ed.* **2008**, *47*, 8848. (b) Luzon, J.; Bernot, K.; Hewitt, I. J.; Anson, C. E.; Powell, A. K.; Sessoli, R. *Phys. Rev. Lett.* **2008**, *100*, 247205/1. (c) Chibotaru, L.; Ungur, L.; Soncini, A. *Angew. Chem., Int. Ed.* **2008**, *47*, 4126. (d) Zaleski, C. M.; Depperman, E. C.; Kampf, J. W.; Kirk, M. L.; Pecoraro, V. L. *Angew. Chem., Int. Ed.* **2004**, *43*, 3912. (e) Aronica, C.; Pilet, G.; Chastanet, G.; Wernsdorfer, W.; Jacquot, J.-F.; Luneau, D. *Angew. Chem., Int. Ed.* **2006**, *45*, 4659. (f) Costes, J.-P.; Shova, S.; Wernsdorfer, W. *Dalton Trans.* **2008**, 1843. (g) Lin, P.-H.; Burchell, T. J.; Ungur, L.; Chibotaru, L. F.; Wernsdorfer, W.; Murugesu, M. *Angew. Chem., Int. Ed.* **2009**, *48*, 9489. (h) Burrow, C. E.; Burchell, T. J.; Lin, P.-H.; Habib, F.; Wernsdorfer, W.; Clérac, R.; Murugesu, M. *Inorg. Chem.* **2009**, *48*, 8051. (i) Gamer, M.; Lan, Y.; Roesky, P. W.; Powell, A. K.; Clérac, R. *Inorg. Chem.* **2008**, *47*, 6581. (j) Zheng, Y.-Z.; Lan, Y.; Anson, C. E.; Powell, A. K. *Inorg. Chem.* **2009**, *47*, 10813. (k) Xu, G.-F.; Wang, Q.-L.; Gamez, P.; Ma, Y.; Clérac, R.; Tang, J.; Yan, S.-P.; Cheng, P.; Liao, D.-Z. *Chem. Commun.* **2010**, *46*, 1506. (l) Langley, S. K.; Moubaraki, B.; Forsyth, C. M.; Gass, I. A.; Murray, K. S. *Dalton Trans.* **2010**, *39*, 1705. (m) Layfield, R. A.; McDouall, J. J. W.; Sulway, S. A.; Tuna, F.; Collison, D.; Winpenny, R. E. P. *Chem.—Eur. J.* **2010**, *16*, 4442.

(4) (a) Coronado, E.; Day, P. *Chem. Rev.* **2004**, *104*, 5419. (b) Bogani, L.; Wernsdorfer, W. *Nat. Mater.* **2008**, *7*, 179.

(5) Milios, C. J.; Vinslava, A.; Wernsdorfer, W.; Moggach, S.; Parsons, S.; Perlepes, S. P.; Christou, G.; Brechin, E. K. *J. Am. Chem. Soc.* **2007**, *129*, 2754.

(6) Chakov, N. E.; Lee, S.-C.; Harter, A. G.; Kuhns, P. L.; Reyes, A. P.; Hill, S. O.; Dalal, N. S.; Wernsdorfer, W.; Abboud, K.; Christou, G. *J. Am. Chem. Soc.* **2006**, *128*, 6975.

(7) Ishikawa, N.; Sugita, M.; Ishikawa, T.; Koshihara, S.; Kaizu, Y. *J. Am. Chem. Soc.* **2003**, *125*, 8694.

(8) Benelli, C.; Gatteschi, D. *Chem. Rev.* **2002**, *102*, 2369.

(9) (a) Van Vleck, J. H. *Phys. Rev.* **1940**, *57*, 426. (b) Van Vleck, J. H. *J. Chem. Phys.* **1939**, *7*, 72.

(10) (a) Orbach, R. *Proc. R. Soc. London, Ser. A* **1961**, *264*, 458. (b) Orbach, R. *Proc. R. Soc. London, Ser. A* **1961**, *264*, 458.

(11) (a) Rinehart, J. D.; Long, J. R. *J. Am. Chem. Soc.* **2009**, *131*, 12558. (b) Rinehart, J. D.; Long, J. R. *J. Am. Chem. Soc.* **2009**, *132*, 7572.

(12) Freedman, D. E.; Harman, W. H.; Harris, T. D.; Long, G. J.; Chang, C. J.; Long, J. R. *J. Am. Chem. Soc.* **2010**, *132*, 1224.

(13) (a) Pearson, R. G. *J. Am. Chem. Soc.* **1963**, *85*, 3533. (b) Pearson, R. G. *J. Chem. Educ.* **1968**, *45*, 581.

(14) (a) Vigato, P. A.; Tamburini, S. *Coord. Chem. Rev.* **2008**, *252*, 1871. (b) Vigato, P. A.; Tamburini, S.; Bertolo, L. *Coord. Chem. Rev.* **2007**, *251*, 1311.

(15) Tang, J.; Hewitt, I.; Madhu, N. T.; Chastanet, G.; Wernsdorfer, W; Anson, C. E.; Benelli, C.; Sessoli, R.; Powell, A. K. *Angew. Chem., Int. Ed.* **2006**, *45*, 1729.

(16) Guo, Y.-N.; Xu, G.-F.; Gamez, P.; Zhao, L.; Lin, S.-Y.; Deng, R.; Tang, J.; Zhang, H.-J. *J. Am. Chem. Soc.* **2010**, *132*, 704422.

(17) Bi, Y.; Wang, X.-T.; Liao, W.; Wang, X.; Deng, R.; Zhang, H.; Gao, S. *Inorg. Chem.* **2009**, *48*, 11743.

(18) Gao, Y.; Xu, G.-F.; Zhao, L.; Tang, J.; Liu, Z. *Inorg. Chem.* **2009**, *48*, 11495.

(19) Guo, Y.-N.; Xu, G.-F.; Gamez, P.; Zhao, L.; Lin, S.-Y.; Deng, R.; Tang, J.; Zhang, H.-J. *J. Am. Chem. Soc.* **2010**, *132*, 8538.

(20) Hussain, B.; Savard, D.; Burchell, T. J.; Wernsdorfer, W.; Murugesu, M. *Chem. Commun.* **2009**, 1100.

(21) Hewitt, I. J.; Lan, Y.; Anson, C. E.; Luzon, J.; Sessoli, R.; Powell, A. K. *Chem. Commun.* **2009**, 6765.

(22) (a) Gu, X.; Xue, D. *Inorg. Chem.* **2007**, *46*, 3212. (b) Gu, X.; Clérac, R.; Houri, A.; Xue, D. *Inorg. Chim. Acta* **2008**, *361*, 3873.

(23) Sheldrick, G. M. *Acta Crystallogr.* **2008**, *A64*, 112.

(24) Wernsdorfer, W. *Supercond. Sci. Technol.* **2009**, *22*, 064013.

(25) Ungur, L.; Van den Heuvel, W.; Chibotaru, L. F. *New J. Chem.* **2009**, *33*, 1224.

(26) Visinescu, D.; Madalan, A. M.; Duhayon, C.; Sutter, J.-P.; Ungur, L.; Van den Heuvel, W.; Chibotaru, L. F.; Andruh, M. *Eur. Chem. J.* **2009**, *15*, 11808.

(27) Chibotaru, L. F.; Ungur, L.; Aronica, C.; Elmoll, H.; Pilet, G.; Luneau, D. *J. Am. Chem. Soc.* **2008**, *130*, 12445.

(28) Karlström, G.; Lindh, R.; Malmqvist, P.-Å.; Roos, B. O.; Ryde, U.; Veryazov, V.; Widmark, P.-O.; Cossi, M.; Schimmelpfennig, B.; Neogrady, P.; Seijo, L. *Comput. Mater. Sci.* **2003**, *28*, 222.

(29) Chibotaru, L. F.; Ungur, L. *The computer programs SINGLE—ANISO and POLY—ANISO*, University of Leuven: Leuven, Belgium, 2006.

(30) Lines, M. E. *J. Chem. Phys.* **1971**, *55*, 2977.

(31) (a) Parr, J.; Ross, A. T.; Slawin, A. M. Z. *Polyhedron* **1997**, *16*, 2765. (b) Dou, W.; Yao, J.-N.; Liu, W.-S.; Wang, Y.-W.; Zheng, J.-R.; Wang, D.-Q. *Inorg. Chem. Commun.* **2007**, *10*, 105. (c) Chakraborty, J.; Thakurta, S.; Samanta, B.; Ray, A.; Pilet, G.; Batten, S. R.; Jensen, P.; Mitra, S. *Polyhedron* **2007**, *26*, 513. (d) Kong, F.-R; Zhang, M. *Chem. J. Chin. Univ.* **1999**, *20*, 839.

(32) Casanova, D.; Llunel, M.; Alemany, P.; Alvarez, S. *Chem.—Eur. J.* **2005**, *11*, 1479.

(33) Kahn, O. *Molecular Magnetism*; VCH: New York, 1993.

(34) Roy, L. E.; Hughbanks, T. *J. Am. Chem. Soc.* **2006**, *128*, 568 and references therein.

(35) Liu, S.; Gelmini, L.; Rettig, S. J.; Thompson, R. C.; Orvig, C. *J. Am. Chem. Soc.* **1992**, *114*, 6081.

(36) Lin, P.-H.; Leclère, M.; Long, J; Burchell, T. J.; Korobkov, I.; Clérac, R.; Murugesu, M. *Dalton Trans.* **2010**, *39*, 5698.

(37) Tang, J.; Hewitt, I.; Madhu, N. T.; Chastanet, G.; Wernsdorfer, W.; Anson, C. E.; Benelli, C.; Sessoli, R.; Powell, A. K. *Angew. Chem., Int. Ed.* **2006**, *45*, 1729.

(38) (a) Cole, K. S.; Cole, R. H. *J. Chem. Soc.* **1941**, *9*, 341. (b) Aubin, S. M. J.; Sun, Z.; Pardi, L.; Krzystek, J.; Folting, K.; Brunel, L. J.; Rheingold, A. L.; Christou, G.; Hendrickson, D. N. *Inorg. Chem.* **1999**, *38*, 5329.

(39) Gatteschi, D.; Sessoli, R.; Villain, J. *Molecular Nanomagnets*; Oxford University Press: New York, 2006 and references therein.

(40) Wernsdorfer, W.; Aliaga-Alcade, N; Hendrickson, D. N.; Christou, G. *Nature* **2002**, *416*, 406.

(41) Aquilante, F.; De Vico, L.; Ferré, N.; Ghigo, G.; Malmqvist, P.-Å.; Neogrády, P.; Pedersen, T. B.; Pitoňák, M.; Reiher, M.; Roos, B. O.; Serrano-Andrés, L.; Urban, M.; Veryazov, V.; Lindh, R. *J. Comput. Chem.* **2010**, *31*, 224.